



## Article

# Precipitation Retrievals from Passive Microwave Cross-Track Sensors: The Precipitation Retrieval and Profiling Scheme

Chris Kidd <sup>1,2,\*</sup> , Toshi Matsui <sup>1,2</sup> and Sarah Ringerud <sup>1,2</sup>

<sup>1</sup> Earth System Science Interdisciplinary Center, University of Maryland, College Park, MD 20740, USA; toshihisa.matsui-1@nasa.gov (T.M.); sarah.e.ringerud@nasa.gov (S.R.)

<sup>2</sup> NASA/Goddard Space Flight Center, Greenbelt, MD 20771, USA

\* Correspondence: chris.kidd@nasa.gov

**Abstract:** The retrieval of precipitation (snowfall and rainfall) from satellite sensors on a global basis is essential in aiding our knowledge and understanding of the Earth System and for many societal applications. Measurements from surface-based instruments are essentially limited to populated regions, necessitating the use of satellite-based observations to provide estimates of precipitation across the whole of the Earth's surface. The temporal and spatial variability of precipitation requires adequate sampling, especially at finer resolutions. It is, therefore, necessary to exploit all available data from precipitation-capable satellites to ensure the proper representation of precipitation. To date, the estimation of precipitation using passive microwave observations has been largely concentrated upon the conically scanning imaging instruments, with relatively few techniques exploiting the observations made from the cross-track sounders. This paper describes the development of the Precipitation Retrieval and Profiling Scheme (PRPS) to retrieve precipitation from cross-track sensors, together with its performance against surface radar data and other satellite precipitation retrievals.



**Citation:** Kidd, C.; Matsui, T.; Ringerud, S. Precipitation Retrievals from Passive Microwave Cross-Track Sensors: The Precipitation Retrieval and Profiling Scheme. *Remote Sens.* **2021**, *13*, 947. <https://doi.org/10.3390/rs13050947>

Academic Editor: Ali Behranghi

Received: 13 February 2021

Accepted: 1 March 2021

Published: 3 March 2021

**Publisher's Note:** MDPI stays neutral with regard to jurisdictional claims in published maps and institutional affiliations.



**Copyright:** © 2021 by the authors. Licensee MDPI, Basel, Switzerland. This article is an open access article distributed under the terms and conditions of the Creative Commons Attribution (CC BY) license (<https://creativecommons.org/licenses/by/4.0/>).

**Keywords:** global precipitation measurement; precipitation retrievals; rainfall; snowfall; validation

## 1. Introduction

Precipitation (rainfall and snowfall) is a crucial element of the global energy and water cycle through the deposition of water from the atmosphere to the Earth's surface [1]. Precipitation also controls the availability of fresh water that is so important to our economic wellbeing and impacting the environment around us through events such as droughts or floods [2]. Despite the importance of precipitation, measurements made by conventional means, such as by rain (and snow) gauges and radar, are generally limited to the more populous regions [3]. Gauges, although essentially providing the de facto measure of precipitation, suffer from systematic biases (e.g., [4]) and may not be representative of the area surrounding the gauge location (see [5,6]). The spatial representation is better addressed in part by using surface-based weather radar, although the radar backscatter to rain-rate (or snow intensity) conversion is not precise, while globally the radar coverage is similar to that of the gauge networks. Most importantly, precipitation varies greatly in time and space, particularly at fine resolutions which are so important to studies of the physical processes associated with precipitation both in the atmosphere and at the surface. Many applications require timely, frequent, and regular measurement of precipitation to capture these variations. For example, the response of a drainage basin generally dictates the temporal sampling of the precipitation necessary to model floods correctly [7], and changes in the duration and intensity of precipitation events and the response of a catchment in a changing climate [8].

The main advantage of satellite-based observations is that they can be used for global precipitation estimation, covering both land and sea, although with differing capabilities. Visible (Vis) and/or Infrared (IR) observations provide frequent and regular observations, particular from geostationary (GEO)-based sensors. While imagery of cloud tops (which

allow measures of reflectivity, cloud top characteristics and cloud top temperature) are useful, the precipitation falling from the base of the cloud must be inferred from these cloud top properties. Consequently, the mainstay of current precipitation observations is based upon passive microwave (PMW) sensors that are sensitive to the hydrometeor particles within and falling from the base of the clouds (see [9]).

A range of PMW instruments have been developed and operated over the last 50 years, the characteristics of which are described in Aonashi and Ferraro [10]. These sensors can be categorised by their observational characteristics and/or scan type. Sensors exploiting the window channels are generally termed “imagers”, while those utilizing absorption bands are termed “sounders”. In the absence of hydrometeors the window channels allow a relatively unrestricted observation of the Earth’s surface, while the latter exploit the differences in the absorption through the atmosphere to extract the vertical distribution of key parameters. Recent satellites carry sensors with both imaging and sounding capabilities to exploit the synergies between the different channels. Sensors can be further categorised by their scan pattern with conically scanning sensors providing observations scribing a cone-shape pattern (allowing consistent Earth incidence angles; EIA) and cross-track sensors whose scan lines are perpendicular to the orbital path of the satellite.

Although cross-track sensors have a relatively long history, their use for the retrieval of precipitation has been secondary to the conically scanning sensors. Challenges relating to their full utilisation include observations that are made at higher frequencies which are not directly related to liquid precipitation at the surface, and their scan geometry which results in varying EIA, footprint size and atmospheric path length at each scan position. The footprint resolution, although ranging from  $20 \times 17$  km at nadir to  $67 \times 28$  km at edge of scan for the Microwave Humidity Sounder (MHS) instrument [11], is comparable with that of some imaging sensors (e.g., Special Sensor Microwave Imager Sounder; SSMIS). While the channel selection of sounders is designed for sounding atmospheric profiles of water vapour and temperature, scattering caused by precipitation-sized hydrometeors provides a means to generate precipitation estimates. Crucially, the inclusion of observations from cross-track sensors into any global precipitation measurement scheme is essential to provide the necessary temporal sampling to capture the variability of precipitation [12]. The Global Precipitation Measurement (GPM) mission [1] includes cross-track sensors as an integral part of the intercalibrated observations from GPM constellation [13]. The current cross-track sensors contributing to the GPM constellation include five MHS sensors [14], two Advanced Technology Microwave Sounder (ATMS) sensors [15], and the Sondeur Atmospherique du Profil d’Humidite Intertropicale par Radiometrie (SAPHIR) sensor [16]: the details of these instruments are outlined in Table 1. Thus, precipitation retrievals from cross-track sensors affects the quality of merged global precipitation rate [17].

**Table 1.** Current operational cross-track sounding instruments with precipitation-retrieval capability. Numbers in brackets indicate number of channels at that specific centre frequency, while V and/or H indicates vertical and/or horizontal polarization.

Sensor	Satellites	Dates	Orbit	Channels	Resolution <sup>1</sup>
MHS	NOAA-18	2005–present	SunSync	89V	$16 \times 16$ km
	NOAA-19	2005–present		157V	
	MetOp-A	2005–present		183.31H(2)	
	MetOp-B	2005–present		190.31V	
	MetOp-C	2005–present			
SAPHIR	Megha-Tropiques	2011–present	NonSunSync	183.31H(6)	$10 \times 10$ km
ATMS	S-NPP NOAA-20	2011–present	SunSync	23.8V, 31.4V, 50.3–57.3H,	$75 \times 75$ km
		2011–present		87–91V, 164–167H,	$32 \times 32$ km
				183.31H(5)	$16 \times 16$ km

<sup>1</sup> Resolution at nadir.

This paper describes the development of a simple, flexible, yet robust algorithm, called the Precipitation Retrieval and Profiling Scheme (PRPS), to retrieve precipitation from cross-track sensors, together with its performance against surface radar data and existing satellite precipitation products.

## 2. Precipitation Retrievals

Alongside the deployment of new PMW sensors has been the development of schemes to retrieve precipitation from their observations. Initial schemes used fundamental characteristics of radiation emitted from raindrops over the oceans to convert the observed brightness temperatures (Tbs) into rain rates. Over land, due to higher background emissivities, higher frequency channels had to be utilised such as the 89 GHz that first flew on the Special Sensor Microwave Imager (SSM/I) from 1987 (see [9]), exploiting the scattering signal caused by precipitation-sized ice particles. Multi-channel retrieval schemes exploit the emission and scattering responses at different frequencies to improve the retrievals, although separate techniques are often required for ocean vs. land retrievals [18]. Radiative transfer modelling (RTM), used to understand the basis of the observed Tbs and improve precipitation retrievals, ranges from relatively simple modelling of Tb-rainrate relationships (see [19]) to inverse RTM to elucidate precipitation associated with the observed signal [20], although many RTM techniques are computationally expensive. To overcome this, many retrieval techniques use a priori databases that are populated with, for example, Tbs from a set of modelled atmospheric profiles (e.g., [21–23]). These database entries are then referenced to best match the observation, providing not only the surface precipitation, but also other modelled parameters used in that database entry. While the original Goddard Profiling (GPROF) scheme (e.g., [24]) envisaged a RTM database, it was clear that the modelled Tbs required adjustments such that the current GPROF database relies upon the combined Dual-frequency Precipitation Radar (DPR)-GPM Microwave Imager (GMI) product to ensure consistency. A similar approach is employed by the retrieval schemes developed by the EUMETSAT Satellite Applications Facility on Support to Operational (H-SAF) for retrievals from both the conically scanning and cross-track scanning radiometers (see [11,25,26]).

The retrieval of precipitation from observations made by PMW sounding instruments was addressed by Surussavadee and Satelin [27] who developed a Mesoscale Model 5 (MM5) model-trained neural network retrieval scheme for Advanced Microwave Sounding Unit (AMSU) observations. The scheme generates a number of atmospheric parameters, including surface precipitation at 15 km resolution across all scan positions. Validation of the products (see [28]) showed good agreement between the satellite and MM5-based retrievals, although problems occurred over Polar or high-altitude regions where column water vapour is minimal. Munchak and Skofronick-Jackson [29] investigated the ability of cross-track sounding instrument sensors to observe and retrieve precipitation by comparing Tropical Rainfall Measuring Mission (TRMM) Microwave Imager (TMI), GMI and AMSUA/B data against radar data over the US. Over the oceans the GMI and TMI performed best due to the availability of the emission-based channels, while the AMSU instruments performed well over land especially when constrained by model information. The higher frequencies of the sounding instruments also respond to the shape and size distribution of the snowflakes [30], although the modelling of the scattering signal associated with complex ice particles these at high frequencies is somewhat problematic [31,32]. Laviola and Levizzani [33] developed the 183-Water-vapour Strong Lines (183-WSL) technique to exploit the observations from the AMSU-B and MHS sensors. Although the constants within the 183-WSL retrieval scheme were critical for the low rain rates and at high latitudes, validation against surface radar over western Europe was encouraging [34].

More recently, the inclusion of the observations from cross-track sensors in the GPM constellation has been crucial to achieve the necessary temporal sampling. Consequently, the GPROF scheme has been adapted to include these observations. The first GPROF cross-track scheme was developed by Kidd et al. [23] using model-derived database entries

to retrieve precipitation from MHS observations. However, in order to better integrate the cross-track observations later versions of GPROF use the DPR-GMI combined observational database, extended to the MHS and ATMS sensors through modelling the different footprint resolutions and frequencies. The cross-track GPROF retrievals use databases segregated by the total precipitable water content (TPW) and the 2m air temperature (T2m) (see [35]), as well as by surface type to mitigate problems arising from the under-constrained nature of the retrieval. The current GPROF scheme was not extended to include observations from the (183 GHz-only) SAPHIR instrument whose current operational retrievals are generated by the PRPS-SAPHIR scheme using a purely observational database but constrained by TPW and T2m.

The EUMETSAT H-SAF has developed a number of precipitation products over the last few years (see [11,36]) based upon the Cloud Dynamics and Radiation Database (CDRD). To ensure consistency, both imager and sounders use the same CDRD physics although conically scanning sensors use a Bayesian retrieval scheme, while cross-track retrievals use the Passive Microwave Neural Network Precipitation Retrieval (PNPR) scheme (see [25]). A more recent version of the PNPR scheme has extended the neural network approach to the conically scanning instruments [26].

The current operational GPROF retrieval scheme, now used for both conically scanning and cross-track sensors, has evolved over the last 20-plus years to process observations from a range of different sensors and incorporate model information to help constrain the retrievals. However, it has a number of disadvantages. First, model information is used to constrain the retrievals by ensuring the correct database entries are assessed at the retrieval stage (see [35]), as well as making the scheme more computationally efficient. However, model data are not available to every developer who might want to test and develop the retrieval technique further. Furthermore, the retrieval scheme becomes model-dependent thus making it less useful for the validation of the model themselves. Second, the GPROF scheme relies upon a single common database generated from coincident combined DPR-GMI observations, from which the databases for individual sensors are generated through modelling the characteristics of the different sensor footprints and frequencies. The "transfer" of information from the single database to the sensor database relies on a number of assumptions and consequently is not perfect, particularly when dealing with the high frequency channels which are often difficult to correctly model the radiation scattering due to the diversity of particle sizes and shapes. Third, the GPROF scheme is computationally intensive, despite having a well thought out strategy for constraining the retrievals. The database is built from over 400 million GMI-DPR observations, which are then grouped into entries with similar characteristics to improve the retrieval efficiency. Finally, the database is built up over a limited period: For GPROF 2017, this was September 2014 through August 2015, during which time it is assumed that the overall characteristics of the database are representative of the periods outside this range. Nevertheless, the GPROF scheme may be considered one of the state-of-the-art schemes against which other retrieval schemes may be compared.

### 3. The Precipitation Retrieval and Profiling Scheme (PRPS)

The PRPS was developed initially for the cross-track sensors using model-rainrate relationships to complement and contribute to the GPROF scheme (see [23]) prior to the launch of the GPM Core Observatory. Results from this early model-based scheme were encouraging, although it was clear that there were differences between modelled and observed Tbs and their derived rain rates. Since the PRPS was developed very much as a test bed to evaluate new approaches it was also developed to more flexible than the GPROF scheme. In particular, the PRPS was built upon three main criteria:

- (i) Avoid the use of dynamic ancillary data, such a model information, snow maps or surface emissivity;
- (ii) Use observational databases to better represent the characteristics of each sensor;

(iii) Be computationally efficient to allow testing of, for example, different channel combinations.

The mechanics of the PRPS is similar to the GPROF retrieval scheme, with the processing effectively split into two: the first step is the generation of the a priori databases that will be used at the retrieval stage, and the second step is the actual retrieval itself where the satellite observations are compared against the a priori database to provide the estimate of precipitation.

### 3.1. The PRPS Database

The key element of the PRPS (and GPROF) is the a priori database against which the observed Tbs are compared and the associated DPR (or combined) rain intensity retrieved. Crucially, the database needs to be representative of the range of precipitation regimes that the sensor will observe. While the GPROF scheme utilises a common GMI-DPR database which is then modelled for the specifics of the other sensors in the GPM constellation, the PRPS generates separate databases based upon matched observations of each sensor and the DPR. This approach has a significant advantage of representing the characteristics and nuances of each sensor type and incorporating the subtle differences between each individual sensor.

An additional feature of the PRPS is that the database is based on a standard  $16 \times 16$  km footprint, derived from  $3 \times 3$  DPR footprints which corresponds to the size of the MHS and ATMS (high resolution) footprints at nadir. Although the resolutions of the cross-track sensors deteriorate towards the edge of swath, the same  $16 \times 16$  km resolution is maintained in the retrieval (similar to the approach of Surussavadee and Staelin [28,29]). While this is not physically correct, the linkage between the  $3 \times 3$  DPR footprints and the associated resolution at a particular scan position is maintained. Moreover, a consistent resolution is more beneficial to the end user than a constantly changing resolution since it maintains the statistical characteristics of the retrieved precipitation, such as frequency of precipitation occurrence.

To generate the a priori database the orbital tracks of the DPR and MHS/ATMS are analysed to find the latitude and longitude of the intersections of their orbits to within 5 min of each other (Figure 1). Note that the actual scan geolocations are used, rather than sub-satellite positions to ensure more precise matchups. This stage outputs the filenames of the MHS/ATMS Level 1C (L1C) data and the DPR Level 2 (L2A) data, together with the date, time, latitude, longitude and distance and bearing of the crossing location. This information is then used to generate the full a priori database from which the operational database will be generated. Data from the following products are included in the full database: (i) L1C MHS/ATMS sensor data, (ii) L1C GMI sensor data, (iii) L2A MHS/ATMS GPROF retrieval, (iv) L2A GMI GPROF retrieval and (v) L2A DPR retrieval. Note that the GMI and GPROF data are only included for comparison and further scientific analysis and is omitted from the operational database. Each of these data product fovs are mapped to a 5 km equal area projection within  $\pm 3000$  km of the orbital crossing location, as shown in Figure 2. The mapping to 5 km ensures that only closely matched footprints are considered in the database. Ancillary data, such as time, geolocation, scan line/position are also included in the data-cube for further analysis and traceability if required. The data-cube is then processed to extract the locations which have coincident footprints across all of the sensor channels and the DPR (the mapped DPR value representing the  $3 \times 3$  mean DPR footprint). Note that since the lower ATMS channels have a lower resolution and slightly different geolocation, they are replicated in adjacent grid boxes to ensure matches with the higher-resolution channels. Table 2 lists the number of MHS/ATMS orbital crossings with the DPR, while Table 3 shows the number of matched MHS/ATMS-DPR footprints by year from 2014 through 2020.

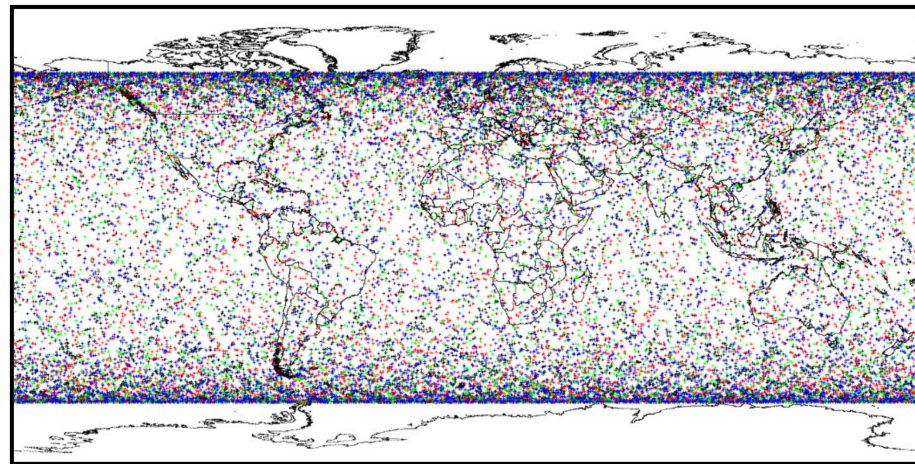


**Figure 1.** Global distribution of the orbital crossing locations between the MHS and the DPR sensors for one year, 2016. The different colours represent the four MHS sensors on MetOp-A (red), MetOp-B (green) NOAA-18 (blue) and NOAA-19 (yellow). Note the latitudinal limit imposed by the coverage of the DPR sensor.

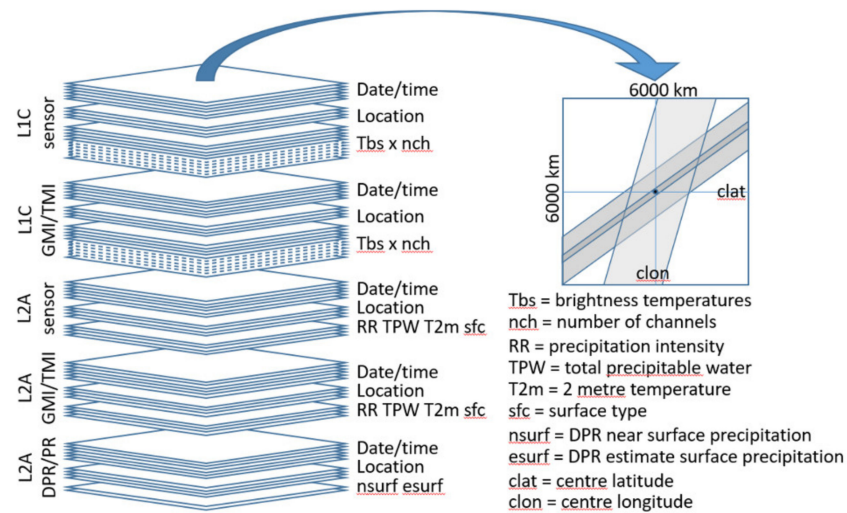


**Figure 2.** Schematic of the datacube generated for each co-incident DPR-sensor orbital crossing. The DPR and the sensor data are mapped onto an equal-area projection centred on the crossing point of the sensors with a resolution of 5 km.

**Table 2.** Number of DPR-MHS/ATMS overpass crossings within 300s of each other by year.

Year	MetOp-A	MetOp-B	MetOp-C	NOAA-18	NOAA-19	NPP	NOAA-20
2014	826	1031	0	1027	1032	1028	0
2015	1333	1333	0	1340	1320	1341	0
2016	1311	1326	0	1319	1326	1347	0
2017	1326	1342	0	1316	1301	1328	111
2018	1320	1319	0	1042	1320	1327	1324
2019	1083	1145	672	0	1107	1323	1328
2020	0	1289	1266	0	1300	1302	1295

**Table 3.** Number of DPR-MHS/ATMS matched footprints obtained from the coincident overpasses by year.

Year	MetOp-A	MetOp-B	MetOp-C	NOAA-18	NOAA-19	NPP	NOAA-20
2014	1,207,022	1,515,746	0	1,505,917	1,509,139	1,440,487	0
2015	1,927,395	1,907,666	0	1,918,439	1,914,316	1,839,842	0
2016	1,965,687	2,000,644	0	1,955,691	1,938,503	1,869,282	0
2017	1,934,333	1,952,317	0	1,903,839	1,878,869	1,875,394	133,677
2018	1,987,148	1,979,471	0	1,556,543	1,929,831	1,825,881	1,832,296
2019	1,548,812	1,626,948	992,100	0	1,665,005	1,904,014	1,908,076
2020	0	1,862,960	1,830,529	0	1,843,978	1,780,979	1,773,997

The output of the datacube for each orbital-match is stored as a text file for ease of reading and checking, and contains a header consisting of the five input filenames followed by the crossing lat/lon and the scale used for the mapping. Following the header each line of text consists of information specific to each sensor, such as the date/time, geolocation, scan position, Tbs for each channel for the L1C data, or the rain retrieval/TPW/T2m/surface type for the L2A data. These data files provide more comprehensive data to enable further analysis, or troubleshooting, of required, and are the basis of the a priori databases that are used in the retrieval scheme.

The full database is then processed and indexed ready for use in the retrieval scheme. To enable the operational database to be loaded into the computer memory (for processing efficiency) only data pertinent to the retrieval process are extracted for inclusion. The key variables are the L1C Tbs, the associated DPR-derived rain rate, scan line/position and the geolocation. To further increase the efficiency of the retrieval, an indexing scheme is used to ensure only the database Tbs close to the observed Tbs are searched. The index is generated first by selecting the most diverse channel combination: in the case of the MHS these are the 150 and  $183 \pm 7$  GHz channels, while for the ATMS 31.4 and  $183 \pm 7$  GHz channels are used. Note that the precise channel selection is not necessarily critical since it only provides a first guess to narrow the initial search. The database is then sorted by the Tbs of these two channels so that at the retrieval stage the index provides a start and end location of the relevant database entries.

Initial studies showed that a large number of database entries is most important in the extreme precipitation situations, but there is essentially little difference between 15M or 30M database entries as long as the entries are representative of the global precipitation systems. Consequently, no fixed size of the databases is currently implemented, but rather the use of all available data with careful quality control screening as necessary.

### 3.2. PRPS Retrieval Methodology

The basic retrieval methodology of the PRPS, like GPROF, is simple: compare the set of observed Tbs with those in the a priori database and select the best match(es). However, the way the comparisons are carried out differ greatly. The GPROF scheme first only considers database entries that match or are close to the values of TPW and T2m as determined by the ancillary model data, and then uses a Bayesian scheme to weight the database entries. Kidd et al. [37] explored different schemes to find the closest database-observation matches, including distance-weighted, Gaussian-weighted and means. Subtle differences were found between the different approaches with no single technique being significantly better than any other.

One of the main challenges of any cross-track retrieval scheme is caused by the cross-track scan pattern that causes variations in EIA, atmospheric path length and footprint size. While the effects of this may be modelled and accounted for within the retrieval scheme, the PRPS scheme takes a simpler approach. Each of the database entries includes the scan position of the original sensor-DPR matchup, therefore only like-scan positions are considered when comparing the observed Tbs with the database Tbs. To avoid limiting the

number of available data entries a scan position range is calculated over which nearby scan positions may also be included. This range is large at the centre of scan where differences between neighbouring scan positions are small and become more restricted towards the end of scan where the differences between adjacent scan positions are greater. To ensure that sufficient database entries per retrieval are available a Tb search parameter is also generated to find a minimum of 10,000 entries within  $\pm 25K$  of the index Tbs. This criterion ensures that where data entries are plentiful (e.g., non-raining values), the search radius is kept small, while in data sparse regions a larger search radius help to ensure a representative number of data entries for the retrieval.

The PRPS calculates the mean of the six closest database entries which was found to be a good compromise between speed and retrieval accuracy [37]. The selection of a number of closest database entries also allows measures of fit between the database and observation Tbs and of the retrieval variability amongst the selected entries. The current scheme outputs the retrieved rain rate, fit and variability based upon the mean of the six database entries, together with the most likely precipitation based upon the closest database entry to the observed Tbs. It should be noted that since the distribution of the rain rates are heavily skewed towards zero this is reflected in any a priori database, and consequently any scheme that combines multiple database entries will underestimate the precipitation intensity in the retrieval.

#### 4. Results

A comparison of the PRPS retrievals against surface reference data from the UKMO European radar composite data is described here. The PRPS retrievals are based upon the methodology described above with the PRPS output providing the geolocation and retrieved precipitation information at a nominal resolution of  $16 \times 16$  km. The surface radar data are available every 15 minutes at a resolution of  $5 \times 5$  km and is therefore averaged to  $15 \times 15$  km by a simple  $3 \times 3$  area moving average to match that of the PRPS retrievals. These retrievals are mapped to the same (Polar Stereographic) projection as the radar data for each overpass and coincident retrieval/radar values are used in subsequent statistical analysis.

A qualitative comparison of the retrievals is shown in Figure 3 with precipitation estimates from the surface radar network together with retrievals from the GPROF and H-SAF PNPR schemes. This case study, using MHS observations from the METOP-A satellite on 13 September 2015 at 20:34 UTC shows a broad area of precipitation over southern France and smaller regions of precipitation over the southern North Sea and western Ireland, as well as a number of isolated precipitation features. The results from the three MHS retrievals are broadly similar to the radar composite, although it can be noted that they vary in intensity and extent. The GPROF retrievals appear to be most similar to the surface radar, although the spatial variability of the GPROF rainfall is somewhat smoother than that of the radar. The H-SAF PNPR product, while identifying the main regions of precipitation, does not identify the small isolated cells, and produces more light precipitation (0.25–0.5 mm/h). The PRPS retrievals appear slightly noisier than the surface radar, although many of the small precipitation features are captured by this scheme.

A quantitative assessment of the retrievals for this case study are shown in Table 4 using four basic statistical and three descriptive measures. It can be seen that the GPROF technique performs best across the statistical scores, followed by the PRPS and then the H-SAF retrievals. For this overpass the (retrieval/reference) ratios are less than one, indicating an underestimation with respect to the surface radar, particularly for the H-SAF technique, while the correlations are generally good. The PRPS generates a mean rain rate closest to the surface radar data (0.43 vs. 0.47 mm/h), although GPROF is closest for the conditional rain rate and the H-SAF technique for the maximum rain rate.

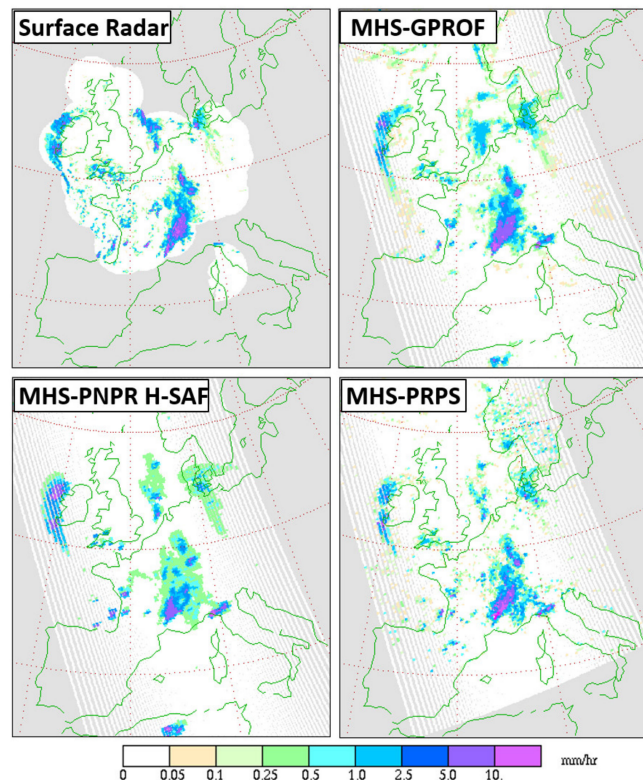


**Figure 3.** Comparison of the surface radar precipitation with retrievals from the MetOp-A MHS observations at 20:34 UTC on 13 September 2015 using GPROF (**top right**), H-SAF (**bottom left**) and the PRPS (**bottom right**).

**Table 4.** Statistical comparison of the MetOp-A MHS retrievals at 20:34 UTC on 13 September 2015.

Statistic	Radar	GPROF	H-SAF	PRPS
Bias	-	−0.02	−0.12	−0.04
Ratio	-	0.944	0.728	0.913
RMSE	-	0.955	1.144	1.500
Correlation	-	0.739	0.585	0.632
Mean rainrate	0.47	0.41	0.31	0.43
Conditional RR	1.21	1.27	1.47	1.58
Maximum RR	16.56	24.46	11.45	41.01

A more comprehensive set of statistical results are shown in Table 5 for the MHS and Table 6 for the ATMS retrievals. To remove issues related to statistical sampling on a case-by-case basis, all the instantaneous retrievals and associated surface data for an entire month and analysed together. For the MHS retrievals, the GPROF technique performs better in terms of the correlation score than the PRPS technique, although the results are more mixed for the ratio. This graphically illustrated in Figure 4 which also compares the statistics of conditional rain rate (both  $\geq 0.2$  mm/h), and thresholded retrievals. Both schemes show significant seasonal variations, with low ratio and correlation scores in the colder seasons: this variation is typical of most PMW retrieval schemes. The results for the ATMS retrievals (Table 6 and Figure 5) show that the GPROF and the PRPS scheme are closer in terms of correlation, but more varied in terms of their ratio. Interestingly, the correlation scores for the GPROF-ATMS are generally lower than those of the GPROF-MHS (0.492–0.606 vs. 0.483–0.667, respectively) and with a small seasonal variation, while the PRPS-MHS scores are consistent (see Tables 5 and 6 below).

**Table 5.** Statistics of instantaneous GPROF and PRPS retrievals for the MetOp-A MHS sensor by month for 2015 over Western Europe.

Year-Month	GPROF				PRPS			
	Bias	Ratio	RMSE	CC	Bias	Ratio	RMSE	CC
2015-01	−0.09	0.425	0.472	0.499	−0.08	0.509	0.521	0.426
2015-02	−0.05	0.483	0.358	0.528	−0.05	0.553	0.416	0.428
2015-03	−0.05	0.498	0.372	0.483	−0.04	0.595	0.402	0.421
2015-04	−0.03	0.523	0.291	0.587	−0.03	0.612	0.325	0.504
2015-05	−0.04	0.624	0.386	0.562	−0.04	0.666	0.429	0.500
2015-06	−0.01	0.868	0.377	0.620	−0.01	0.800	0.489	0.520
2015-07	−0.02	0.808	0.445	0.607	−0.02	0.782	0.493	0.571
2015-08	0.00	0.967	0.555	0.632	−0.02	0.872	0.680	0.551
2015-09	−0.02	0.796	0.400	0.667	−0.02	0.735	0.488	0.566
2015-10	−0.02	0.783	0.379	0.619	−0.02	0.716	0.422	0.545
2015-11	−0.06	0.604	0.442	0.528	−0.06	0.578	0.492	0.449
2015-12	−0.06	0.574	0.479	0.563	−0.07	0.540	0.513	0.499

**Table 6.** Statistics of instantaneous GPROF and PRPS retrievals for the NPP-ATMS sensor by month for 2015 over western Europe.

Year-Month	GPROF				PRPS			
	Bias	Ratio	RMSE	CC	Bias	Ratio	RMSE	CC
2015-01	−0.09	0.415	0.472	0.506	−0.09	0.434	0.491	0.519
2015-02	−0.06	0.434	0.352	0.492	−0.05	0.454	0.359	0.463
2015-03	−0.05	0.448	0.363	0.509	−0.05	0.511	0.381	0.500
2015-04	−0.04	0.442	0.298	0.522	−0.04	0.438	0.287	0.502
2015-05	−0.04	0.652	0.392	0.550	−0.04	0.685	0.430	0.517
2015-06	−0.01	0.790	0.338	0.563	−0.03	0.649	0.362	0.554
2015-07	−0.02	0.820	0.465	0.603	−0.02	0.814	0.509	0.560
2015-08	−0.01	0.904	0.543	0.606	−0.03	0.784	0.566	0.571
2015-09	−0.02	0.771	0.454	0.592	−0.03	0.651	0.492	0.565
2015-10	−0.01	0.907	0.379	0.596	−0.03	0.676	0.377	0.573
2015-11	−0.06	0.601	0.451	0.527	−0.07	0.557	0.507	0.493
2015-12	−0.07	0.562	0.493	0.560	−0.07	0.543	0.477	0.539

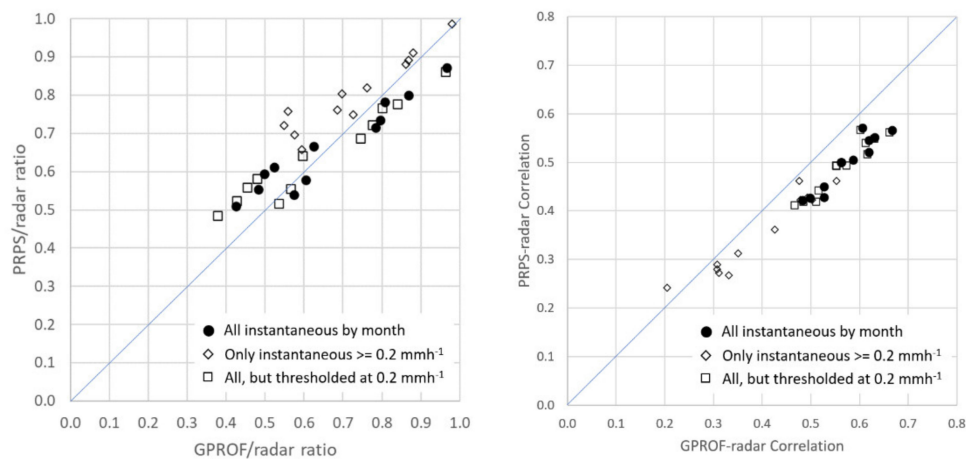


**Figure 4.** Comparison of PRPS and GPROF statistics for quantitative assessment of instantaneous retrievals over Western Europe during 2015 for the MetOp-A MHS sensor. Each dot presents 1 month of instantaneous statistical analysis. Scatterplot on left compares the ratios (retrieval/observed) while the right scatterplot compares the correlation (retrieval wrt observed). Filled circles are for all instantaneous comparisons by month, diamonds are for only where both retrieval and observed were  $\geq 0.2$  mm/h, while the squares threshold the rain intensity at 0.2 mm/h (the nominal minimum detectable rain rate of the DPR).

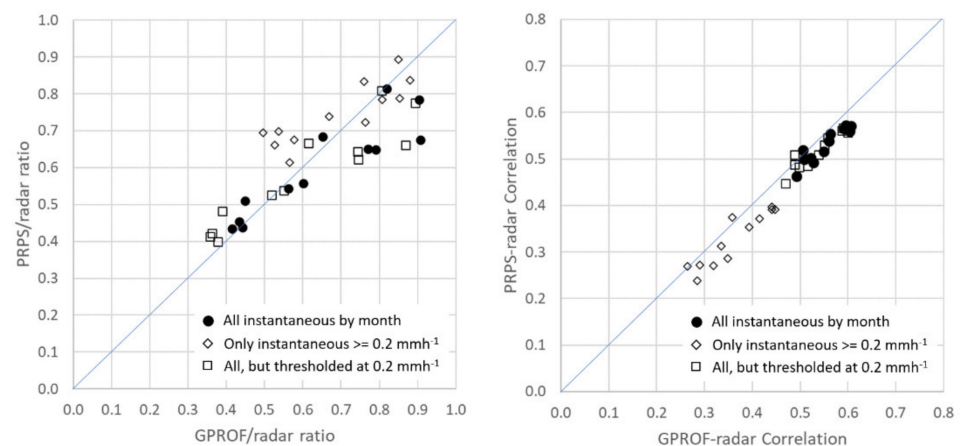


**Figure 5.** As Figure 4 above but for the NPP-ATMS sensor.

## 5. Discussion

The PRPS described above is primarily designed as a straightforward retrieval scheme that associates the precipitation observed by the GPM DPR with the Tbs observed by a particular sensor. In particular, the scheme does not use any channel weightings, surface background information or dynamic/model ancillary data. The scheme relies upon the information content contained within the observations to provide model-independent precipitation estimates. The absence of the additional information makes the PRPS scheme more flexible and computationally faster. The PRPS also provides precipitation estimates at a constant resolution, which although for cross-track sensors is not necessarily physically correct, provides the user with a consistent precipitation product that allows easier integration into multi-satellite precipitation products.

Although the performance of the PRPS is generally lower than that of GPROF, it does well at identifying and retrieving precipitation. There is clearly a trade-off between algorithm complexity and improvements in the final retrieval. The PRPS compares the observed Tbs with those in the database with no additional information, whereas GPROF uses a Bayesian scheme to select the database entries which are constrained by surface type, model TPW and T2m. In addition, GPROF uses a hybrid a priori database comprised

of both DPR (combined) observations and entries derived from the surface based MRMS radar data. Another major drawback of a complex retrieval scheme is one of traceability: the PRPS allows the user to find the source of the original database entry, and therefore the “context” of that particular entry, while the multi-stage elements of the GPROF scheme makes this much more difficult.

The better performance of the GPROF scheme may in part be due to the information provided by the model (TPW and T2m) to constrain the retrieval. Clearly the more information that is available at the retrieval stage, the better the retrieval should be. The current official NASA retrieval scheme for the SAPHIR cross-track sensor uses the PRPS-SAPHIR which does incorporate the model data used by the GPROF scheme, primarily since the SAPHIR is a single frequency, 6-channel radiometer and therefore has limited channel diversity: the additional model information is required to enable sensible retrievals to be made. However, the greater channel diversity of the MHS and the ATMS allows more information to be extracted from the observations themselves. This may, in part, explain why the PRPS retrievals from the ATMS are better (in terms of correlation) than those from the MHS, particularly with the inclusion of the 23 and 31 GHz channels on the ATMS. The correlation performance of the GPROF and PRPS ATMS retrievals suggest that given sufficient channel diversity, surface type and model information may not actually be critical. Exploratory studies using PRPS scheme on GMI data (with 13 channels) suggests that the retrievals match, or even exceed those of the GPROF scheme. This initial work also highlights one of the main issues using the DPR-derived precipitation in the database since the DPR cannot see shallow precipitation or precipitation close to the surface since the minimum retrievable altitude is about 1500 m above the surface.

Future work on the PRPS is ongoing with the aim of improving the retrievals from the cross-track sensors through better representation of the rainfall in the databases. Retrievals from additional cross-track sensors, such as the Feng-Yun (FY)-3C Micro-Wave Humidity Sounder (MWHS)-2 and Time-Resolved Observations of Precipitation structure and storm Intensity with a Constellation of Smallsats (TOPICS) are also being evaluated at present. Expansion of the PRPS to conically scanning sensors is also underway with encouraging initial results. While the algorithm described above outlines the “retrieval” part of the scheme, the full PRPS also has a proofing capability, as demonstrated by Kidd [38]. The full implementation of this has not been fully realised since it is computationally more expensive due to handling 120 levels, rather than just the surface data. The PRPS profiling element uses the a priori database to refer back to the original L2A DPR data so the profile information from the DPR can be included if needed. Initial comparisons of the closest profile associated with the set of Tb observations, was shown to compare well with the coincident DPR observations. This section is not mandatory but can be added to the manuscript if the discussion is unusually long or complex.

## 6. Conclusions

The PRPS has been designed to invoke one of the key goals of the GPM mission: to use the instrumentation on the GPM Core Observatory as a transfer standard to other sensors within the GPM constellation. The PRPS utilises the rainfall information from the DPR (or DPR-GMI combined) to generate an a priori database against which observations from the cross-track sensors may be compared to retrieve a rain rate. A key goal of the PRPS was to reduce, or eliminate, the dependence of the retrieval scheme on external data sets, especially dynamic/model data sets that might require special access or privileges. While undoubtedly the inclusion of these external data sets provides additional information that is deemed useful in the retrievals, much of this information is already present in the satellite observations, particularly for observations made by diverse-frequency sensors such as the GMI. For the cross-track sensors although the PRPS does not meet the overall performance of the GPROF scheme, it does show considerable merit, particularly with the ATMS sensor with the greater range of channels than the MHS. In particular, the lack

of model information within the retrieval scheme makes it a truly independent source of precipitation information against which models may be compared.

**Author Contributions:** Conceptualization and methodology were carried out by C.K. and T.M.; validation, formal analysis by C.K.; investigation by C.K. and S.R.; writing—original draft preparation, C.K.; writing—review and editing, C.K., T.M. and S.R.; visualization, C.K.; funding acquisition, C.K., T.M. and S.R. All authors have read and agreed to the published version of the manuscript.

**Funding:** Research funding for this paper was provided in part through NASA Award Number, 80NSSC19K0825xxx as part of the NASA Precipitation Measurement Missions.

**Institutional Review Board Statement:** Not applicable.

**Informed Consent Statement:** Not applicable.

**Data Availability Statement:** The source data for this study are openly available from <https://gpm.nasa.gov/data/directory>.

**Acknowledgments:** The authors wish to thank the NASA Precipitation Processing System for provision of data and UK BADC/CEDA for the surface radar data. The authors would also like to acknowledge the anonymous reviewers of the paper and appreciate their feedback and suggestions.

**Conflicts of Interest:** The authors declare no conflict of interest.

## References

1. Hou, A.Y.; Kakar, K.K.; Neeck, S.A.; Azarbarzin, A.; Kummerow, C.D.; Kojima, M.; Oki, R.; Nakamura, K.; Iguchi, T. The global precipitation measurement mission. *Bull. Am. Meteorol. Soc.* **2014**, *95*, 701–722. [[CrossRef](#)]
2. Skofronick-Jackson, G.; Petersen, W.A.; Berg, W.; Kidd, C.; Stocker, E.F.; Kirschbaum, D.B.; Kakar, R.; Braun, S.A.; Huffman, G.J.; Iguchi, T.; et al. The Global Precipitation Measurement (GPM) mission for science and society. *Bull. Am. Meteorol. Soc.* **2017**, *98*, 1679–1695. [[CrossRef](#)]
3. Kidd, C.; Huffman, G.; Becker, A.; Skofronick-Jackson, G.; Kirschbaum, D.; Joe, P.; Muller, C. So, how much of the Earth's surface is covered by rain gauges? *Bull. Am. Meteorol. Soc.* **2017**, *98*, 69–78. [[CrossRef](#)]
4. Duchon, C.E.; Biddle, C.J. Undercatch of tipping-bucket gauges in high rain rate events. *Adv. Geosci.* **2010**, *25*, 11–15. [[CrossRef](#)]
5. Sevruk, B.; Zhlavova, L. Classification system of precipitation gauge site exposure: Evaluation and application. *Int. J. Climatol.* **1994**, *14*, 681–689. [[CrossRef](#)]
6. Sevruk, B. Regional dependency of precipitation-altitude relationship in the Swiss Alps. *Clim. Change* **1997**, *36*, 355–369. [[CrossRef](#)]
7. Reed, P.M.; Chaney, N.W.; Herman, J.D.; Ferringer, M.P.; Wood, E.F. Internationally coordinated multi-mission planning is now critical to sustain the space-based rainfall observations needed for managing floods globally. *Environ. Res. Lett.* **2015**, *10*, 024010. [[CrossRef](#)]
8. Merz, B.; Aerts, J.; Arnbjerg-Nielsen, K.; Baldi, M.; Becker, A.; Bichet, A.; Blöschl, G.; Bouwer, L.M.; Brauer, A.; Cioffi, F.; et al. Floods and climate: Emerging perspectives for flood risk assessment and management. *Nat. Hazards Earth Syst. Sci.* **2014**, *14*, 1921–1942. [[CrossRef](#)]
9. Kummerow, C.D. Introduction to passive microwave retrieval methods. In *Satellite Precipitation Measurement*; Levizzani, V., Kidd, C., Kirschbaum, D.B., Kummerow, C.D., Nakamura, K., Turk, F.J., Eds.; Springer Nature: Cham, Switzerland, 2020; Volume 67, pp. 123–140. [[CrossRef](#)]
10. Aonashi, K.; Ferraro, R.R. Microwave sensors, imagers and sounders. In *Satellite Precipitation Measurement*; Levizzani, V., Kidd, C., Kirschbaum, D.B., Kummerow, C.D., Nakamura, K., Turk, F.J., Eds.; Springer Nature: Cham, Switzerland, 2020; Volume 67, pp. 63–81. [[CrossRef](#)]
11. Mugnai, A.; Casella, D.; Cattani, E.; Dietrich, S.; Laviola, S.; Levizzani, V.; Panegrossi, G.; Petracca, M.; Sano, P.; Di Paola, F.; et al. Precipitation products from the hydrology SAF. *Nat. Hazards Earth Syst. Sci.* **2013**, *13*, 1959–1981. [[CrossRef](#)]
12. Chambon, P.; Roca, R.; Jobard, I.; Capderou, M. The Sensitivity of Tropical Rainfall Estimation from Satellite to the Configuration of the Microwave Imager Constellation. *IEEE Trans. Geosci. Remote Sens. Lett.* **2013**, *10*, 996–1000. [[CrossRef](#)]
13. Wilheit, T.; Berg, W.; Ebrahimi, H.; Kroodsma, R.; McKague, R.; Payne, V.; Wang, J. Intercalibrating the GPM constellation using the GPM microwave imager. In Proceedings of the IEEE International Geoscience and Remote Sensing Symposium (IGARSS), Milan, Italy, 26–31 July 2015.
14. NOAA/NASA. NOAA, 2014: NOAA KLM User's Guide. Available online: <https://www1.ncdc.noaa.gov/pub/data/satellite/publications/podguides/N-15%20thru%20N-19/pdf/0.0%20NOAA%20KLM%20Users%20Guide.pdf> (accessed on 14 September 2020).
15. Kim, E.; Lyu, C.-H.J.; Anderson, K.; Leslie, R.V.; Blackwell, W.J. S-NPP ATMS instrument prelaunch and on-orbit performance evaluation. *J. Geophys. Res. Atmos.* **2014**, *119*, 5653–5670. [[CrossRef](#)]

16. Gohil, B.S.; Gairola, R.M.; Mathur, A.K.; Varma, A.K.; Mahesh, C.; Gangwar, R.K.; Pal, P.K. Algorithms for retrieving geophysical parameters from the MADRAS and SAPHIR sensors of the Megha-Tropiques satellite: Indian scenario. *Q. J. Roy. Meteorol. Soc.* **2013**, *139*, 954–963. [[CrossRef](#)]
17. Huffman, G.J.; Bolvin, D.T.; Braithwaite, D.; Hsu, K.-L.; Joyce, R.J.; Kidd, C.; Nelkin, E.J.; Sorooshian, S.; Stocker, E.F.; Tan, J.; et al. Integrated Multi-satellite Retrievals for the Global Precipitation Measurement (GPM) Mission (IMERG). In *Satellite Precipitation Measurement*; Levizzani, V., Kidd, C., Kirschbaum, D.B., Kummerow, C.D., Nakamura, K., Turk, F.J., Eds.; Springer Nature: Cham, Switzerland, 2020; Volume 67, pp. 343–353. [[CrossRef](#)]
18. Weng, F.; Ferraro, R.R.; Grody, N.C. Global precipitation estimations using Defense Meteorological Satellite Program F10 and F11 special sensor microwave imager data. *J. Geophys. Res.* **1994**, *99*, 14493–14502. [[CrossRef](#)]
19. Olson, W.S. Physical retrieval of rainfall rates over the ocean by multispectral microwave radiometry: Application to tropical cyclones. *J. Geophys. Res.* **1989**, *94*, 2267–2280. [[CrossRef](#)]
20. Cotton, W.R.; Tripoli, G.J. Numerical-simulation of the effects of varying ice crystal nucleation rates and aggregation processes on orographic snowfall. *J. Clim. Appl. Meteorol.* **1986**, *25*, 1658–1680. [[CrossRef](#)]
21. Tripoli, G.J.; Cotton, W.R. A numerical investigation of several factors contributing to the observed variable intensity of deep convection over south Florida. *J. Appl. Meteorol.* **1980**, *19*, 1037–1063. [[CrossRef](#)]
22. Kummerow, C.D.; Randel, D.L.; Kulie, M.; Wang, N.; Ferraro, R.; Munchak, S.J.; Petkovic, V. The Evolution of the Goddard Profiling Algorithm to a Fully Parametric Scheme. *J. Atmos. Ocean. Technol.* **2015**, *32*, 2265–2280. [[CrossRef](#)]
23. Kidd, C.; Matsui, T.; Chern, J.; Mohr, K.; Kummerow, C.; Randel, D. Global Precipitation Estimates from cross-track passive microwave observations using a physically based retrieval scheme. *J. Hydrometeorol.* **2016**, *17*, 383–400. [[CrossRef](#)]
24. Kummerow, C.D.; Ringerud, S.; Crook, J.; Randel, D.; Berg, W. An Observationally Generated A Priori Database for Microwave Rainfall Retrievals. *J. Atmos. Ocean. Technol.* **2011**, *28*, 113–130. [[CrossRef](#)]
25. Sanò, P.; Panegrossi, G.; Casella, D.; Di Paola, F.; Milani, L.; Mugnai, A.; Petracca, M.; Dietrich, S. The Passive microwave Neural network Precipitation Retrieval (PNPR) algorithm for AMSU/MHS observations: Description and application to European case studies. *Atmos. Meas. Technol.* **2015**, *8*, 837–857. [[CrossRef](#)]
26. Sanò, P.; Panegrossi, G.; Casella, D.; Marra, A.C.; D’Adderio, L.P.; Rysman, J.F.; Dietrich, S. The Passive Microwave Neural Network Precipitation Retrieval (PNPR) Algorithm for the CONICAL Scanning Global Microwave Imager (GMI) Radiometer. *Remote Sens.* **2018**, *10*, 1122. [[CrossRef](#)]
27. Surussavadee, C.; Staelin, D.H. Global Millimeter-Wave Precipitation Retrievals Trained With a Cloud-Resolving Numerical Weather Prediction Model, Part I: Retrieval Design. *IEEE Trans. Geosci. Remote Sens.* **2008**, *46*, 99–108. [[CrossRef](#)]
28. Surussavadee, C.; Staelin, D.H. Global Millimeter-Wave Precipitation Retrievals Trained With a Cloud-Resolving Numerical Weather-Prediction Model, Part II: Performance Evaluation. *IEEE Trans. Geosci. Remote Sens.* **2008**, *46*, 109–118. [[CrossRef](#)]
29. Munchak, S.J.; Skofronick-Jackson, G. Evaluation of precipitation detection over various surfaces from passive microwave imagers and sounders. *Atmos. Res.* **2013**, *131*, 81–94. [[CrossRef](#)]
30. Skofronick-Jackson, G.M.; Johnson, B.T.; Munchak, S.J. Detection Thresholds of Falling Snow From Satellite-Borne Active and Passive Sensors. *IEEE Trans. Geosci. Remote Sens.* **2013**, *51*, 4177–4189. [[CrossRef](#)]
31. Brogniez, H.; English, S.; Mahfouf, J.F.; Behrendt, A.; Berg, W.; Boukabara, S.; Buehler, S.A.; Chambon, P.; Gambacorta, A.; Geer, A.; et al. A review of sources of systematic errors and uncertainties in observations and simulations at 183 GHz. *Atmos. Meas. Technol.* **2016**, *9*, 2207–2221. [[CrossRef](#)]
32. Fox, S.; Mendrok, J.; Eriksson, P.; Ekelund, R.; O’Shea, S.J.; Bower, K.N.; Baran, A.J.; Harlow, R.C.; Pickering, J.C. Airborne validation of radiative transfer modelling of ice clouds at millimetre and sub-millimetre wavelengths. *Atmos. Meas. Technol.* **2019**, *12*, 1599–1617. [[CrossRef](#)]
33. Laviola, S.; Levizzani, V. The 183-WSL fast rain rate retrieval algorithm: Part I: Retrieval design. *Atmos. Res.* **2011**, *99*, 443–461. [[CrossRef](#)]
34. Laviola, S.; Levizzani, V.; Cattani, E.; Kidd, C. The 183-WSL fast rain rate retrieval algorithm. Part II: Validation using ground radar measurements. *Atmos. Res.* **2013**, *134*, 77–86. [[CrossRef](#)]
35. Berg, W.; L’Ecuyer, T.; Kummerow, C. Rainfall Climate Regimes: The Relationship of Regional TRMM Rainfall Biases to the Environment. *J. Appl. Meteorol. Clim.* **2006**, *45*, 434–454. [[CrossRef](#)]
36. Mugnai, A.; Smith, E.A.; Tripoli, G.J.; Bizzarri, B.; Casella, D.; Dietrich, S.; Di Paola, F.; Panegrossi, G.; Sanò, P. CDRD and PNPR satellite passive microwave precipitation retrieval algorithms: EuroTRMM/EURAINSAT origins and H-SAF operations. *Nat. Hazards Earth Syst. Sci.* **2013**, *13*, 887–912. [[CrossRef](#)]
37. Kidd, C.; Ringerud, S.; Skofronick-Jackson, G.; Huffman, G. Precipitation retrievals from passive microwave cross-track sounding instruments. In Proceedings of the 14th Specialist Meeting on Microwave Radiometry and Remote Sensing of the Environment (MicroRad), Espoo, Finland, 11–14 April 2016; pp. 107–109. [[CrossRef](#)]
38. Kidd, C. Defining a simple 3D precipitation retrieval scheme. In Proceedings of the 8th International Precipitation Working Group Meeting, Bologna, Italy, 3–7 October 2016; Available online: [http://ipwg.isac.cnr.it/meetings/bologna-2016/Bologna2016\\_Posters/P1-15\\_Kidd.pdf](http://ipwg.isac.cnr.it/meetings/bologna-2016/Bologna2016_Posters/P1-15_Kidd.pdf) (accessed on 2 March 2021).